Supporting Information

Mineral nanoparticle aggregation alters contaminant transport under flow

Lian Zhou[1], Laurent Lassabatere[2], N. Tan Luong[3], Jean-François Boily[3], Khalil Hanna[1]*

[1]Univ Rennes, Ecole Nationale Supérieure de Chimie de Rennes, UMR CNRS 6226, 11 Allée de Beaulieu, F-35708 Rennes Cedex 7, France.

[2] Univ Lyon, Université Claude Bernard Lyon 1, CNRS, ENTPE, UMR5023 LEHNA Vaulx-en-Velin, France.

[3]Department of Chemistry, Umeå University, Umeå, SE-901 87, Sweden.

29 Pages, 11 Figures, 4 Tables.

Materials. All reagents were purchased from Sigma-Aldrich and used without further purification. All solutions were prepared with ultrapure water and no contact with glass surfaces during preparation to prevent silica contamination. A 1-mM stock solution of nalidixic acid (NA) was prepared by dissolving 1-mmol NA in 20 mL of 1-M NaOH and then diluted with 1 L of ultrapure water. A similar approach was used to make a stock of 1-mM niflumic acid (NFA). The stock solutions of dissolved silicate (Si) (1 mM, 2 mM) were prepared from $Na_2SiO_3 \cdot 9H_2O$ dissolved in 0.01-M NaCl. According to Halasz *et al.*,[1] where 80% of the species were monomeric in solutions of 0.2 M $Na_2SiO_3 \cdot 9H_2O$, polymeric species likely represent a very small proportion of the 1–2-mM silicate solutions used in this work. A 0.1 mM dissolved phosphate (P) stock solution was made from NaH_2PO_4, which had the same 0.01-M NaCl as the background electrolyte concentration. Quartz sand from Fontainebleau (100–300 μm) was purchased from VWR Prolabo (France). The sand was washed with HCl and H_2O_2 and then with ultrapure water several times to remove impurities**.**

Synthesis and Characterization of Goethite (α-FeOOH). Goethite was synthesized as described in previous study.[2] 400 mL of 2.5 mol L^{-1} sodium hydroxide solution was added to 500 mL of 0.5 mol/L ferric nitrate solution ($Fe(NO_3)_3 \cdot 9H_2O$) at a fixed rate of 9 mL/min with stirring and in a nitrogen atmosphere. The obtained hydroxide slurry was aged at 60 °C for 72 h in an oven. The precipitate obtained was dialyzed (Spectra/Por membrane 2) against Milli-Q water. Water was then changed every day until its conductivity was below 0.5 μS/cm. The suspensions were thereafter stored in polypropylene containers at 4 °C. The purity of goethite was confirmed by X-ray diffraction (XRD). The Brunauer, Emmett, and Teller (BET) specific surface area of the synthetic goethite was 91±1 m^2/g.

The point of zero charge (PZC) of goethite, determined at 298 K in 0.01 , 0.1, and 1 M NaCl solutions by the potentiometric titration method, was 9.1. Our previous TEM investigations showed that goethite particles are acicular–i.e., between 200 and 400 nm long and between 100 and 200 nm wide.

Synthesis and characterization of goethite aggregates. Goethite aggregates were synthesized by freezing-thawing method,[3] as follows. We first froze a freshly-shaked and 500 mL goethite suspension (2 g/L) in high-density polyethylene container in a freezer at −20 °C. After 3 weeks, the frozen goethite was allowed to thaw at 4 °C, producing goethite aggregates. To obtain a relatively coarse aggregate shape, the freezing and thawing temperatures were chosen according to a previous work.[3] After removing the supernatant to obtain the goethite aggregates, we dried the goethite aggregates in an oven at 60 °C. XRD and BET data showed that freezing-thawing and drying did not affect the crystal structure or the specific surface area of goethite. The size distribution of pores (Figure S1) in goethite aggregates was evaluated by applying the Barrett–Joyner–Halenda (BJH) method (assuming cylindrical pore shape) to the N_2 gas desorption isotherm data.

Water vapor adsorption and desorption measurements were conducted to check the effects of aggregation on the distribution of hydroxo-groups of the goethite surface. The results (Figure S2) confirmed no modification of the distribution of hydroxo groups between normal goethite and aggregated goethite.

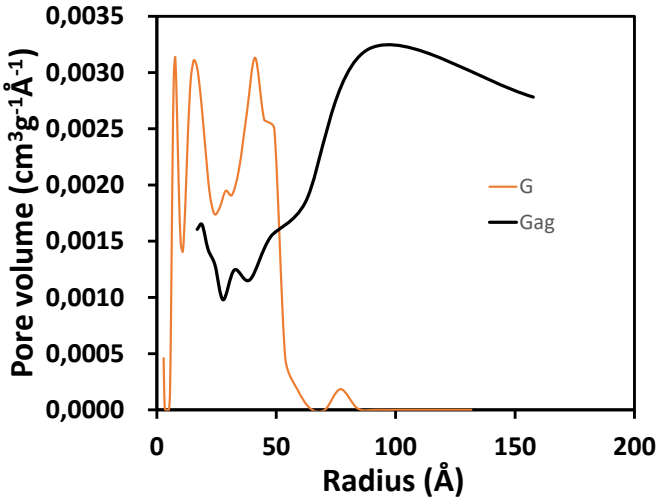

Figure S1. Pore volume distribution of goethite and goethite aggregates evaluated by applying the Barrett–Joyner–Halenda (BJH) method to the N_2 gas desorption isotherm data.

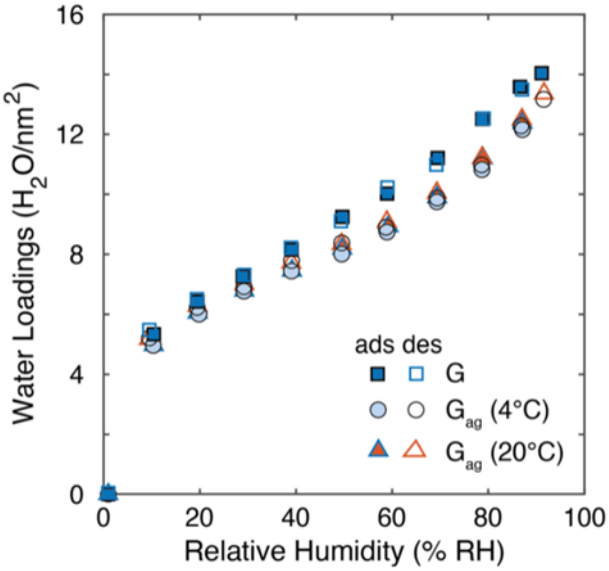

Figure S2. Water loadings on goethite particles and two kinds of goethite aggregates.

Synthesis of GCS and G_{ag}CS. Fontainebleau quartz sand (with particle size range of 100−300 μm) was used to synthesize GCS following previous studies.[2,4,5] Goethite coating was obtained by shaking a suspension containing the goethite and the silica sand. The purified quartz sand was then added to the goethite suspension containing 10 mM NaCl brought to pH 5 with HCl and the mixture was agitated again for 24 h. After that, the coated sand was washed with deionized water until the runoff was clear, and then it was dried for 24 h. The final goethite-coated sand was stored at ambient temperature until further use. The goethite content deposited on the sand surface, measured by acid digestion analysis, was 1 g/100 g of sand. G_{ag}CS was synthesized by mixing 0.15 g of dried goethite aggregates with 14.85 g of clean quartz sand, using the same protocol as described above. According to acid digestion analysis, goethite content in GCS and G_{ag}CS was 1 ± 0.02 wt%.

Control tests have been done with the bare sand to check whether the uncoated sand may contribute to the adsorption of target compounds investigated in this study. All results showed that the adsorption of organic (NA , NFA) or inorganic (P, Si) compounds is negligible on the Fontainebleau quartz sand (150-300 μm, 0.06 m^2/g) used here. In addition, injection of reactive solutes in uncoated sand columns provides the same breakthrough behavior, as for bromide tracer, thus confirming the well-known inert nature of the Fontainebleau quartz sand.

The quartz sand (100-300 μm) was used here as an inert support for goethite in column tests. These coated sand materials are generally used as a structurally stable and hydraulically conductive porous medium to mimic natural mineral assemblages. The inert nature of the Fontainebleau quartz sand used in this study and its very high stability (or its very low solubility) was verified experimentally here. Furthermore, the possible dissolution of the used quartz sand was, additionally checked in 1 and 10

g/L sand suspensions that were continuously stirred over a range of pH values (4-10) in pure water or 0.01 M NaCl for up to one month. In all cases, the dissolved silicate concentrations were below the detection limit of the molybdenum blue spectrophotometric method (<1 µM) and ICP-AES (<0.2 µM).

ATR-FTIR investigations. The ATR-FTIR data suggests that NA binds to goethite through metal-bonded (MB), H-bonded (HB), and outer-sphere (OS) complexes, as shown in our previous work.[6] The bands at 1706 cm^{-1} found in $NA_{(s)}$ correspond to the C=O stretching mode of the protonated carboxylic group. These bands disappear in solution and at the goethite surface while two other bands appear, corresponding to $\nu_{COO,as}$ ($NA_{(aq)}$: 1578 cm^{-1}) and $\nu_{COO,s}$ ($NA_{(aq)}$: 1392 cm^{-1}). Almost 25 cm^{-1} blue shifts in C-O stretching modes (ν_{COO}) was observed with no obvious shift for the ring modes ν_{ring}, suggesting direct interactions of carboxyl groups with goethite but little interaction with the aromatic and pyridine rings. No significant effect of pH on adsorbed NA or NFA is observed for 4 < pH < 6.

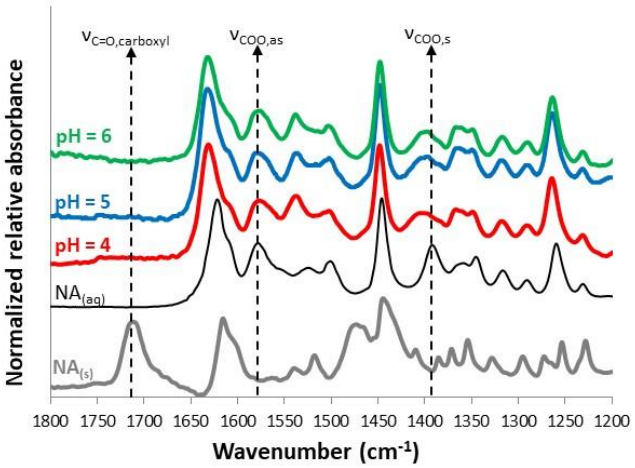

Figure S3. ATR-FTIR spectra at different pH values. Comparison between $NA_{(aq)}$, $NA_{(s)}$ and goethite-NA at pH = 4, 5 and 6.

Surface complexation modeling. Surface complexation modeling was done with geochemical speciation code PHREEQC-2.[7] The charge-distribution multisite complexation (CD-MUSIC) model[8] was used to calculate surface species of two organic ligands (NA and NFA) and two oxyanions (Si and P) on goethite. In a previous study,[6] we showed that NA binds to goethite through metal-bonded (MB), H-bonded (HB), and outer-sphere (OS) complexes. NFA had a weak affinity on goethite, binding only through OS complexes. However, sorption of NFA increased in the NA-NFA-goethite system because of co-binding of an OS complex of NFA onto NA bound to goethite through MB, HB, or OS complexes, as we have previously shown.[6] Si binding from solutions of monomeric Si species first produced monomeric MB complexes resulting from a ligand exchange reaction with singly coordinated hydroxo ($\equiv FeOH^{-0.5}$) groups when at Si loadings below ~1 Si/nm^2.[9] At Si surface loadings exceeding ~1 Si/nm^2, oligomerization and polymerization reactions occurred when monomer silicates attach to existing MB Si species.[9] As phosphate has a high affinity on goethite, it can form monodentate complexes and bidentate complexes at goethite surfaces.[10] The surface complexation reactions of all surface species are reported in Table S1.

The charge of the goethite/water interface was treated using the three-plane model (TPM). Charges of the adsorbates were distributed among the 0 (H^+, MB), 1 (HB), and 2 (Na^+, Cl^-, OS) planes of the TPM. According to the MUSIC model approach,[11] singly ($\equiv FeOH^{-0.5}$), doubly ($\equiv Fe_2OH$), and triply ($\equiv Fe_3O^{-0.5}$ and $\equiv Fe_3OH^{+0.5}$) coordinated sites outcrop the goethite surface, depending on the crystal face. A simplified 1-pK surface charging model, neglecting the contributions of doubly- and part of the triply-coordinated sites, was used. The reactive site density is detailed in our previous work[5]: $[\equiv FeOH^{-0.5}] = 3.12$ sites/nm^2 and $[\equiv Fe_3O^{-0.5}] = 3.12$ sites/nm^2 on (001)/(101) planes (90% of the surface

area) and [≡$FeOH^{-0.5}$] = 7.4 sites/nm² on (210)/(010) plane (10% of the surface area). The protonation constants of these groups were set to pH_{pzc} (1-pK approximation approach of MUSIC model). All the calculations used the "minteq v4" database.

Surface complexation modeling combined with kinetics. Since surface complexation model (SCM) describes sorption based on surface reaction equilibrium, this method could be applied when surface reactions reached local equilibrium or, at least, were not significantly affected by chemical nonequilibrium. When non-equilibrium conditions prevailed, implementation of kinetics in surface complexation reactions was needed. NA can form MB, HB and OS complexes as follows according to ATR-FTIR data (Figure S3):

$$2H^+ + 2{\equiv}FeOH^{-0.5} + NA^- \rightleftharpoons (\equiv FeOH_2)_2^+ \cdots NA^- \quad \text{(OS complexes)} \qquad \text{(S1.1)}$$

$$2H^+ + 2{\equiv}FeOH^{-0.5} + NA^- \rightleftharpoons (\equiv FeOH_2)_2^+ \cdots NA^- \quad \text{(HB complexes)} \qquad \text{(S1.2)}$$

$$2H^+ + 2{\equiv}FeOH^{-0.5} + NA^- \rightleftharpoons (\equiv Fe)_2(NA^0) + 2H_2O \quad \text{(MB complexes)} \qquad \text{(S1.3)}$$

Fast formation of OS complexes is a prerequisite for IS complex formation, which is a rate-limiting process due to the conversion of hydrogen-bonded organic species to metal-bonded complexes. To distinguish the two-step reactions in PHREEQC-2, we have applied a two-step surface reaction expression. Briefly, we defined one intermediate 'NA^{in}' and one equilibrium 'NA' species. Here, 'NA^{in}' is an intermediate complex first in the form of an OS species:

$$2H^+ + 2{\equiv}FeOH^{-0.5} + NA^{in-} \rightleftharpoons (\equiv FeOH_2)_2^+ \cdots NA^{in-} \quad \text{(OS formation)} \qquad \text{(S1.4)}$$

It then converts to a HB species through:

$$2H^+ + 2{\equiv}FeOH^{-0.5} + NA^{in-} \rightleftharpoons (\equiv FeOH_2)_2^+ \cdots NA^{in-} \quad \text{(HB formation)} \qquad \text{(S1.5)}$$

The resulting HB species then converts to a MB through:

$$(\equiv FeOH_2)_2^{+}\cdots NA^{in-} \quad (HB) \underset{K_b}{\overset{K_f}{\rightleftarrows}} (\equiv Fe)_2(NA^0) + 2H_2O \quad (MB) \qquad (S1.6)$$

K_f and K_b are forward and backward rate coefficients (T^{-1}) respectively, which could be obtained by curve fitting.

To describe adsorption kinetics of Si and P on goethite, we propose a multiple-site equilibrium/kinetic surface reaction expression, which was modified from a two-site equilibrium/kinetic sorption model[12] and a multi-rate surface reaction expression.[13] The equilibrium sorption sites assumes that surface reactions were instantaneous. For kinetic sorption sites, multiple first-order rate constants are used to describe the macroscopic rate of sorption, as follows:[13]

$$\frac{\partial m^{\mathrm{k}}}{\partial t} = \alpha^{k}\left(Q^{\mathrm{k}} - m^{k}\right),\ \mathrm{k} = 1, 2, \ldots, M, \qquad (S1.7)$$

Here, m^{k} and Q^{k} are the concentration (M/L^3) and adsorption extent (M) of sorbed chemical component at sorption site k normalized to aqueous volume, and α^{k} is the first-order sorption rate constant (T^{-1}) of target chemical at kinetic sorption site k, which was obtained by curve fitting according to experimental data. The adsorption extent of each chemical component was calculated based on surface complexation reactions in section 2.5 at reaction equilibrium. Here, the distributed rate expression in the original work[13] was simplified to multiple first-order rate constants.

Table S1. Surface complexation reactions and charge distribution of NA species, silicate species, and phosphate species on goethite in the CD-MUSIC model*.

Reaction	Type	log K	Δz0	Δz1	Δz2
$\equiv Fe_3O^{-0.5} + H^+ \rightleftharpoons \equiv Fe_3OH^{+0.5}$		9.1 [a]	1	0	0
$\equiv Fe_3O^{-0.5} + H^+ + Cl^- \rightleftharpoons \equiv Fe_3OH^{+0.5}\cdots Cl^-$		8.1 [b]	1	0	-1
$\equiv Fe_3O^{-0.5} + Na^+ \rightleftharpoons \equiv Fe_3OH^{+0.5}\cdots Na^+$		-1 [c]	0	0	1
$\equiv FeOH^{-0.5} + H^+ \rightleftharpoons \equiv FeOH_2^{+0.5}$		9.1 [a]	1	0	0
$\equiv FeOH^{-0.5} + H^+ + Cl^- \rightleftharpoons \equiv Fe_3OH^{+0.5}\cdots Cl^-$		8.1 [b]	1	0	-1
$\equiv FeOH^{-0.5} + Na^+ \rightleftharpoons \equiv FeOH^{-0.5}\cdots Na^+$		-1 [c]	0	0	1
$2H^+ + 2\equiv FeOH^{-0.5} + NA^- \rightleftharpoons (\equiv Fe)_2(NA^0) + 2H_2O$	MB	19.7 [d]	1	0	0
$2H^+ + 2\equiv FeOH^{-0.5} + NA^- \rightleftharpoons (\equiv FeOH_2)_2^+\cdots NA^-$	HB	20 [d]	2	-1	0
$2H^+ + 2\equiv FeOH^{-0.5} + NA^- \rightleftharpoons (\equiv FeOH_2)_2^+\cdots NA^-$	OS	20.8 [d]	2	0	-1
$3H^+ + 2\equiv FeOH^{-0.5} + NFA^- \rightleftharpoons (\equiv FeOH_2)_2^+\cdots NFAH$	HBH	27[d]	+2	0	0
$2H^+ + 2\equiv FeOH^{-0.5} + NFA^- \rightleftharpoons (\equiv FeOH_2)_2^+\cdots NFA^-$	OS	19.9 [d]	+2	0	-1
$2H^+ + 2\equiv FeOH^{-0.5} + NFA^- + Na^+ \rightleftharpoons (\equiv FeOH_2)_2^+\cdots NFA^-\cdots Na^+$	HB-Na	20.8[d]	+2	-1	1
$2H^+ + 2\equiv FeOH^{-0.5} + NA^- + NFA^- \rightleftharpoons (\equiv Fe)_2(NA^0)\cdots (NFA)^- + 2H_2O$	MB-OS	23.2 [d]	+1	0	-1
$2H^+ + 2\equiv FeOH^{-0.5} + NA^- + NFA^- \rightleftharpoons (\equiv FeOH_2)_2^+\cdots (NA)\cdots (NFA)^-$	HB-OS	23.2[d]	+2	-1	-1
$2H^+ + 2\equiv FeOH^{-0.5} + NA^- + NFA^- \rightleftharpoons (\equiv FeOH_2)_2^+\cdots (NA)\cdots (NFA)^-$	OS-OS	25.4[d]	+2	0	-2
$2H^+ + 2\equiv FeOH^{-0.5} + NA^- + NFA^- + Na^+ \rightleftharpoons (\equiv FeOH_2)_2^+\cdots (NA)\cdots (NFA)^-\cdots Na^+$	HB-HB-Na	26.3[d]	+2	-2	+1
$2\equiv FeOH^{-0.5} + Si(OH)_4^0 \rightleftharpoons (\equiv FeO)_2Si(OH)_2^- + 2H_2O$	MB	5.85[e]	0.48	-0.48	0
$2\equiv FeOH^{-0.5} + 2H^+ + PO_4^{-3} \rightleftharpoons (\equiv FeO)_2PO_2^{-2} + 2H_2O$	MB	28.31 [f]	0.46	-1.46	0
$\equiv FeOH^{-0.5} + 2H^+ + PO_4^{-3} \rightleftharpoons \equiv FeOPO_2OH^{-1.5} + H_2O$	MB	26.36 [f]	0.28	-1.28	0

*TPM with C_1 = 2.3 F/m^2, C_2 = 1.07 F/m^2; 63% of (101), 27% of (001), and 10% of (210). Site densities: [$\equiv FeOH^{-0.5}$] = 3.03, 3.34, and 7.4 site/nm^2 at the (101), (001), and (210) planes, respectively; [$\equiv Fe_3O^{-0.5}$] = 3.03 and 3.34 site/nm^2 at the (101) and (001) planes, respectively. All types of surface species are considered to form at all planes ((101)/(001)/(210)). All other parameters were fixed.

[a] Values from F. Gaboriaud, J.-J. Ehrhardt, Effects of different crystal faces on the surface charge of colloidal goethite (α-FeOOH) particles: an experimental and modeling study, Geochimica et Cosmochimica Acta. 67 (2003) 967–983.[2]

[b] Values from T. Hiemstra, W.H. Van Riemsdijk, On the relationship between charge distribution, surface hydration, and the structure of the interface

of metal hydroxides, Journal of Colloid and Interface Science. 301 (2006) 1–18. [14]

[c] Values from R.P.J.J. Rietra, T. Hiemstra, W.H. van Riemsdijk, Electrolyte Anion Affinity and Its Effect on Oxyanion Adsorption on Goethite, Journal of Colloid and Interface Science. 229 (2000) 199–206.[15]

[d] Values from Xu, J.; Marsac, R.; Wei, C.; Wu, F.; Boily, J.-F.; Hanna, K. . Environ. Sci. Technol. 2017, 51 (20), 11617–11624.[16]

[e] Values from Hiemstra, T.; Barnett, M. O.; van Riemsdijk, W. H. [9]Interaction of Silicic Acid with Goethite. J. Colloid Interface Sci. 2007, 310 (1), 8–17. [17]

[f] Values from Rahnemaie, R.; Hiemstra, T.; van Riemsdijk, W. H. Geometry, Charge Distribution, and Surface Speciation of Phosphate on Goethite. Langmuir 2007, 23 (7), 3680–3689. [10]

Analysis and modeling of tracer breakthrough curves (BTCs). The columns may contain isolated water, in addition to mobile water and immobile water fractions. The isolated water fraction corresponds to pockets of stagnant water that are not accessible to solutes. The computation of moments and the modeling with mobile-immobile model (MIM) are used to complete the determination of the isolated, immobile and mobile water fractions, along with the solute mass exchange between the mobile and immobile water fractions. The isolated water fractions may involve water in the core of aggregates that are not easily accessible and that can be considered as utterly isolated. Mass balances and retardation factors were calculated using the zero- and first-order moments of the BTCs obtained from tracer experiments. The absolute time moments are defined by[18]

$$\mu_{\mathrm{n}} = \int_0^{+\infty} t^{\mathrm{n}} C(t)\, dt, \mathrm{n} = 0, 1, 2, \cdots, N \qquad \text{(S2.1)}$$

where $C(t)$ is the effluent concentrations (M/L^3) at time t, μ_{n} is the nth order absolute time moment. μ_0 is the zeroth absolute time moment and is proportional to the total mass that is being eluted from the column. The mass balance ratio can be computed by dividing the zeroth order moment by the product inlet concentration multiplied by the duration of the pulse injection. The retardation factor R was calculated as the ratio of the mean tracer residence time (T_{m}) to the theoretical water resident time (T_{s}), which represents the time needed to replenish water in the column. The mean residence time of solute and retardation factor can be calculated as follows[19,20]:

$$T_{\mathrm{m}} = \frac{\mu_1}{\mu_0} - \frac{\delta_{\mathrm{t}}}{2}, T_{\mathrm{s}} = \frac{L \cdot \theta_{total}}{q}, R = \frac{T_{\mathrm{m}}}{T_{\mathrm{s}}} \qquad \text{(S2.2)}$$

Where δt is the duration of pulse injection (T), L and θ are the length (L) and volumetric total water content (L^3/L^3) of the column, and q is the Darcian velocity (L/T).

After obtaining the isolated water fraction, tracer transport in GCS and $G_{ag}CS$ columns was modelled on the basis of the classical advection-dispersion equation (ADE) and the mobile-immobile model (MIM) implemented in the HYDRUS-1D code[21]. The governing equation of ADE for a non-reactive solute in one-dimensional systems could be derived as follows (considering steady and uniform flow in the columns):

$$\theta \frac{\partial C}{\partial t} = -\theta v \frac{\partial C}{\partial x} + \theta D_{\mathrm{h}} \frac{\partial^2 C}{\partial x^2} \qquad \text{(S2.3)}$$

where C is the concentration of solute at position x (M/L^3), t is time (T), θ is the volumetric water content (L^3/L^3). D_{h} is hydrodynamic dispersion coefficient (L^2/T), v is the average pore velocity (L/T). The concept of MIM model assumes that there are two regions in pore space, namely mobile zone (macropores or inter-aggregate pores) and immobile zone (micropores or intra-aggregate pores).[19] Rapid transport in the mobile water is accompanied by diffusive mass transfer of solutes between the mobile and immobile water fractions. The governing equations read as follows for a nonreactive solute, considering an homogeneous and constant water flow[22]:

$$\theta_{\mathrm{m}} \frac{\partial C_{\mathrm{m}}}{\partial t} + \theta_{\mathrm{im}} \frac{\partial C_{\mathrm{im}}}{\partial t} = -\theta_{\mathrm{m}} v_{\mathrm{m}} \frac{\partial C_{\mathrm{m}}}{\partial x} + \theta_{\mathrm{m}} D_{\mathrm{m}} \frac{\partial^2 C_m}{\partial x^2} \qquad \text{(S2.4}a\text{)}$$

$$\theta_{\mathrm{im}} \frac{\partial C_{\mathrm{im}}}{\partial t} = \omega (C_{\mathrm{m}} - C_{\mathrm{im}}) \qquad \text{(S2.4b)}$$

$$\theta = \theta_{\mathrm{im}} + \theta_{\mathrm{m}} \qquad \text{(S2.4}c\text{)}$$

where θ_{m} and θ_{im} are the volumetric water content (L^3/L^3) in the mobile and immobile region respectively, C_{im} and C_{m} are the solute concentrations in the immobile and mobile region respectively (M/L^3), v_{m} is the pore water velocity in the mobile region (L/T), D_{m} is the hydrodynamic dispersion coefficient in the mobile region (L^2/T), ω is the mass transfer coefficient between the mobile and immobile regions (T^{-1}). In both ADE and MIM model, the hydrodynamic dispersion coefficient is

related to the pore velocity and the molecular diffusion coefficient D_0 (L^2/T) through:

$$D_{\mathrm{h}} = \lambda v + \tau D_0, \qquad D_{\mathrm{m}} = \lambda_{\mathrm{m}} v_{\mathrm{m}} + \tau D_0 \qquad \text{(S2.5)}$$

Where λ is the longitudinal dispersivity (L) and τ is the tortuosity (dimensionless), m and im subscripts refer to "mobile" and "immobile" water fractions.

The set of equations (S2.3-S2.5) were resolved numerically using HYDRUS-1D code for the tracer. In ADE approach, the only fitting hydrodynamic parameter was the longitudinal dispersivity (λ). In MIM, four fitting hydrodynamic parameters should be determined, including the mobile and immobile water fractions (θ_{m}, θ_{im}), the longitudinal dispersivity (λ_{m}) and the mass transfer coefficient (ω). These values can be optimized with HYDRUS inverse procedure considering weighting by standard deviation.

On the basis of the hydrodynamic parameters, it is possible to estimate the characteristic times relative to the physical processes that drive the solute transport: advection and dispersion in the mobile zone, diffusion at the interface between the mobile and immobile water fraction, diffusion into the immobile water fraction. The advection time (T_{adv}) corresponds to the mean time nonreactive solutes should spend in the column in case no exchange occurs between the mobile and the immobile fractions. The mass transfer time T_{ω} quantifies the kinetics of the solute exchange between the two types of water. The comparison of this time to the advection time gives an idea of the magnitude of the exchange relative to advection. These characteristic times are calculated by the following relations:

$$T_{\mathrm{adv}} = \frac{L \cdot \theta_{\mathrm{m}}}{q} \qquad T_{\omega} = \frac{\theta_{\mathrm{im}}}{\omega} \qquad \text{(S2.6)}$$

During water saturation, tracer experiments and reactive transport tests, fractions were collected from the column effluent and acidified in order to measure possible mobilized FeOOH particles. In all samples, the total dissolved Fe in the outflow was below the ICP-AES detection limit (0.2 µM for Fe), and therefore the possibility of mobilization of goethite particles can be excluded.

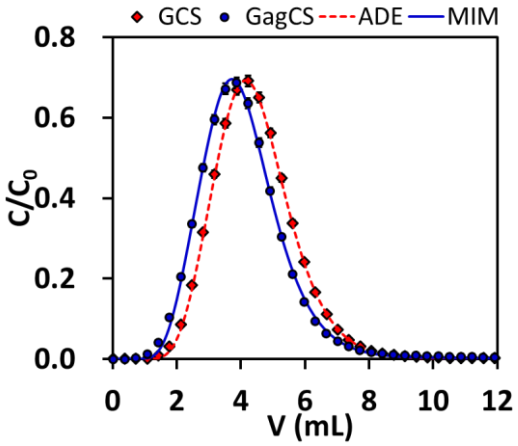

Figure S4. Experimental and modeled BTCs of Br^- at constant flow rate of 0.5 mL/min in GCS and $G_{ag}CS$ columns. The points correspond to the experimental data. Lines corresponds to the best models, with the solid line and dashed line corresponding to the fits to $G_{ag}CS$ and GCS BTCs using MIM and ADE, respectively.

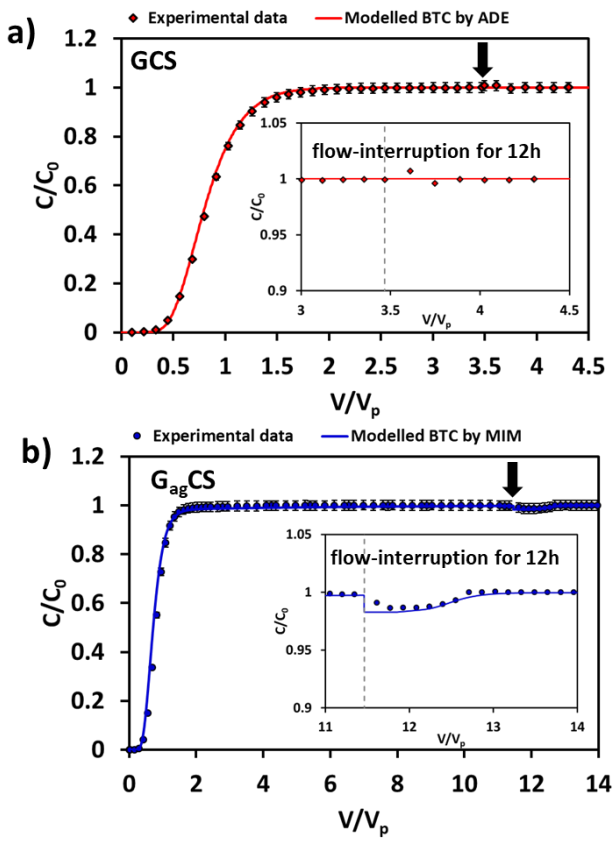

Figure S5. Experimental and modeled BTCs of Br^- in flow-interruption experiments performed in GCS (a) and $G_{ag}CS$ columns (b). Inflow conditions for the two sets of experiment: flow rate 0.5 mL/min, 0.05-M NaBr prepared with 0.01-M NaCl background electrolyte, inflow pH 5.0 ± 0.1, 12-hour flow-interruption. The points represent the observed data. The solid lines are the modeled BTCs. The arrows and the dashed lines indicate the stop-flow points. Embedded subfigure: zoom in after recommencing flow.

Figure S4 illustrates the experimental and modeled BTCs of bromide in GCS and $G_{ag}CS$ columns. According to the results from the zero- and first-order moment analyses of the experimental BTCs, the mass balance ratios in both GCS and $G_{ag}CS$ columns were close to 100% (in the range of 97.1%~99.9%) and the retardation factors were 84.7% ±1.3% in GCS columns and 85.3±0.7% in $G_{ag}CS$ columns. The

slightly lower than unity retardation factors reveal an exclusion of bromide anion from part of the water in both types of columns. This exclusion may have resulted from the presence of completely isolated water (such as water trapped in isolated and unconnected pores) in addition to anionic exclusion. However, we consider anionic exclusion as negligible because surface charge of goethite is positive at pH5. Thus, in this case, retardation factors can be used to quantify the fraction of isolated water by the following relation[19,23]:

$$\theta_{is} = (1\text{-}R) \cdot \theta \qquad \text{(S2.7)}$$

The isolated water fraction is removed from the total water content for data modeling. Then, the experimental BTCs are fitted to the numerical model, using Hydrus-1D in inverse mode. In GCS columns, the ADE provided the best fit (goodness of fit, R^2=0.999), suggesting relatively homogeneous flow in the column. The obtained hydrodynamic parameters show that 15.3% of the total water volume is completely isolated and the immobile water fraction can be ignored. In G_{ag}CS columns, the best fit was obtained with the MIM (R^2=0.998), suggesting that the water is fractionated into mobile and immobile water fractions. The hydrodynamic parameters show that the flow concerned 76.0% of the total water volume and the rest was either immobile (9.8%) or completely isolated (14.2%). The determined mass transfer rate constant ω is 1.48×10^{-3} min^{-1} (0.089 h^{-1}) which falls in the typical range (0.03 ~ 0.09 h^{-1}) according to previous studies[13,24] at similar scales and for similar experimental conditions. The exchange between the mobile and the immobile fractions was not instantaneous insofar as the mass transfer time (T_{ω}= 31.4 min) is longer than the advection time (T_{adv}= 6.2 min). Retardation Factors, hydrodynamic parameters and characteristic times for columns of GCS and G_{ag}CS are summarized in Table S2.

The discrepancy of flow regimes in GCS and $G_{ag}CS$ columns were also confirmed by the independent sets of flow-interruption experiments with step-injection of bromide in GCS and $G_{ag}CS$ columns (Figure S5). No drop in the Br^- BTC suggested the immobile water fraction can be ignored in GCS columns, whereas the relative concentration dropped to ~0.97 after flow-interruption in $G_{ag}CS$ columns, indicating diffusive mass transfer between mobile and immobile regions. Using corresponding hydrodynamic parameters in Table S2, the experimental Br^- BTCs in both GCS and $G_{ag}CS$ columns can be well predicted by ADE and MIM, respectively.

Table S2. Retardation Factors (R), hydrodynamic parameters and characteristic times for columns of goethite coated sand (GCS) and goethite aggregate coated sand ($G_{ag}CS$) [a]

Column	R (%)	f_{is} (%)	T_m (min)	Hydrodynamic parameters in ADE or MIM					T_{adv} (min)	T_ω (min)
GCS	84.7 (1.3)	15.3 (1.60)	7.1 (0.1)	ADE	θ (-) 0.361(0.007)	λ (cm)* 0.243(0.005)			7.1 (0.1)	-
$G_{ag}CS$	85.7 (0.7)	14.2 (1.7)	6.94 (0.06)	MIM	θ_m (-)* 0.322 (0.007)	θ_{im}(-)* 0.042 (0.017)	λ_m(cm)* 0.325 (0.012)	ω(min^{-1})* 1.48e-3 (0.51e-3)	6.2 (0.1)	31.4 (12.5)

[a] Mean (standard deviations)

* Parameters obtained from curve-fitting

Reactive transport modeling. To model reactive solute transfer under dynamic conditions, we coupled the transport module with surface complexation model considering both equilibrium and non-equilibrium reactions in PHREEQC-2. The transport module allows the simulation of convection and dispersion in relation with either advection-dispersion equation (ADE) or mobile-immobile model (MIM) approaches. For ADE, aqueous concentrations of target chemicals are governed by the following advection-reaction-dispersion (ARD) equation:[7]

$$\frac{\partial C}{\partial t} = -v\frac{\partial C}{\partial x} + D_L\frac{\partial^2 C}{\partial x^2} - \frac{\partial q}{\partial t}, \quad \text{(S3.1)}$$

where C is concentration in water (M/L^3), t is time (T), v is mean pore water flow velocity (L/T), x is distance (L), D_L is hydrodynamic dispersion coefficient (L^2/T), and q is concentration in the solid phase normalized to aqueous volume (expressed as M/L^3). The chemical interaction term $\frac{\partial q}{\partial t}$, calculated separately from the transport part for each time step, is the sum of all equilibrium and non-equilibrium reaction rates. Similarly, the mass transport of a reactive solute in MIM can be expressed as follows:[13]

$$\theta_m\frac{\partial C_m}{\partial t} = -\theta_m v_m\frac{\partial C_m}{\partial x} + \theta_m D_m\frac{\partial^2 C_m}{\partial x^2} - \omega\theta_{im}(C_m - C_{im}) - \theta_m\frac{\partial q_m}{\partial t} \quad \text{(S3.2a)}$$

$$\frac{\partial C_{im}}{\partial t} + \frac{\partial q_{im}}{\partial t} = \omega(C_m - C_{im}), \quad \text{(S3.2b)}$$

where θ_m and θ_{im} are the volumetric water content (L^3/L^3) in the mobile and immobile region, respectively, C_{im} and C_m are solute concentrations in the immobile and mobile region, respectively (M/L^3), q_m and q_{im} are concentrations in the solid phase located in the immobile and mobile region (M/L^3), v_m is mean pore water velocity in the mobile region (L/T), D_m is hydrodynamic dispersion coefficient in the mobile region (L^2/T), and ω is the mass transfer coefficient between the mobile and immobile regions (T^{-1}). The chemical interaction terms $\frac{\partial q_m}{\partial t}$ and $\frac{\partial q_{im}}{\partial t}$ are the sum of all equilibrium and non-equilibrium reaction rates in the immobile and mobile region, respectively. Moreover, we distributed the sorption sites linked to goethite between the mobile and immobile water fractions. This distribution can be described by parameter f (%), which is the fraction of sorption sites in contact with mobile water.

Transport modeling was performed with the geochemical model PHREEQC-2. The numerical approach in PHREEQC-2 follows the basic components of mass transport equations in a split-operator scheme.[7] Fate and transport parameters were estimated by fitting the model solution to the experimental BTC for the reactive solute only (i.e., not for pH).

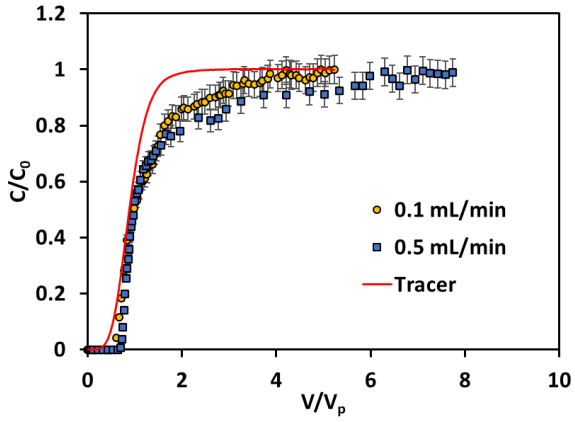

Figure S6. BTCs of NA normalized by its retardation factor to that of the bromide (tracer), at two flow rates. Inflow conditions: 10 μM NA, 0.01 M NaCl, PV=3.7 ± 0.1 mL, inflow pH=5 ± 0.1. The red solid is BTC of bromide, and the points represent the observed data.

Sensitivity analysis of mass transfer coefficient ω and fraction of sorption sites in contact with mobile water, *f*. In order to investigate how mass transfer coefficient ω and fraction *f* affect the shape of BTCs for NA, sensitivity analyses of parameter ω and *f* were performed using PHREEQC-2. The sensitivity analysis of the mass transfer coefficient ω (T^{-1}) was conducted with a series of values between 0.09 h^{-1} (the values obtained from tracer test) and 4.32 h^{-1} in combination with a fixed value of fraction *f* (10%). Following similar method, sensitivity analysis of parameter *f* was performed with a series of values between 0% and 100% in combination with a fixed value of the mass transfer coefficient ω (4.32 h^{-1}). Based on the results from sensitivity analyses, we found parameter α and *f* can be independently determined by curve-fitting: *f* mainly governs the position of initial breakthrough point, whereas ω determines the turning point of relative concentration where the tailing starts.

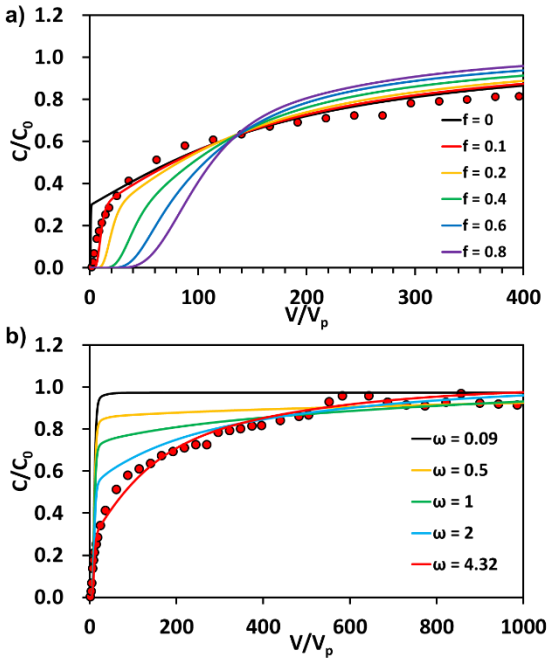

Figure S7. Sensitivity analysis of mass transfer coefficient ω (a) and fraction *f* (b) based on breakthrough experiment of NA in G_{ag}CS column. Influent solutions of 10 µM NA were injected in step-type concentration boundary condition. Inflow conditions: flow rate 0.5 mL/min, 10 mM NaCl background electrolyte inflow pH 5.0 ± 0.1. Pore volumes is 4.1± 0.1 mL. The solid lines are modeled BTCs for NA obtained by using PHREEQC-2. The points correspond to the experimental data.

Table S3. Parameters in the model setup with explicit approach by using PHREEQC-2

Parameters	GCS columns				G_{ag}CS columns		
	NA	Si	PO_4 (with NA)	NFA (with NA)	NA	Si	PO_4 (with NA)
Column length (cm)	4.9 ± 0.1				4.9 ± 0.1		
Effective porosity (-)	0.36				0.36		
Mean pore velocity (cm/h)	41.33				41.21		
Dispersivity (cm)	0.243 ± 0.005				0.325 ± 0.012		
Bulk density (g/cm^3)	1.55 ± 0.05				1.55 ± 0.05		
Porosity ratio: θ_{im}/θ_m (-)	-				9.7%		
Mass transfer coefficient (h^{-1})	-				4.32		
Type of kinetic expression for surface complexation reactions	Two-step kinetics	Multi-site	Multi-site	-	Two-step kinetics	Multi-site	Multi-site
Percentage of kinetic sorption sites	-	50% [a]	100%[a]	0% [b]	-	100% [b] (MD*) 90% [b] (ID#)	100% [b] (MD) 100% [b] (ID)
First-order kinetic rate constant (h^{-1})	K_f = 0.05 [c] K_b = 0.009 [c]	1.80 [b]	0.24 [b]	-	K_f = 0.05 [c] K_b = 0.009 [c]	0.6 (MD) 0.6 (IM)	0.72 [b] (MD) 0.06 [b] (MD)

*MD represents Mobile Domain.

#ID represents Immobile Domain.

[a]Parameters were obtained by curve-fitting.

[b]The percentage of kinetic sorption sites equaling 0 means all the sorption sites are assumed to be equilibrium.

[c]Values from Zhou, L.; Cheng, W.; Marsac, R.; Boily, J.-F.; Hanna, K. Silicate Surface Coverage Controls Quinolone Transport in Saturated Porous Media. Journal of Colloid and Interface Science 2022, 607, 347–356.[25]

Table S4. Parameters in the model setup with implicit approach by using PHREEQC-2

Parameters	G_{ag}CS columns		
	NA	Si	NA & NFA
Column length (cm)	4.9 ± 0.1		
Effective porosity (-)	0.36		
Mean pore velocity (cm/h)	41.21		
Dispersivity (cm)	0.325 ± 0.012		
Bulk density (g/cm^3)	1.55 ± 0.05		
Porosity ratio: θ_{im}/θ_m (-)	9.7%		
Overall mass transfer coefficient (h^{-1})	2.35	0.05	1.44

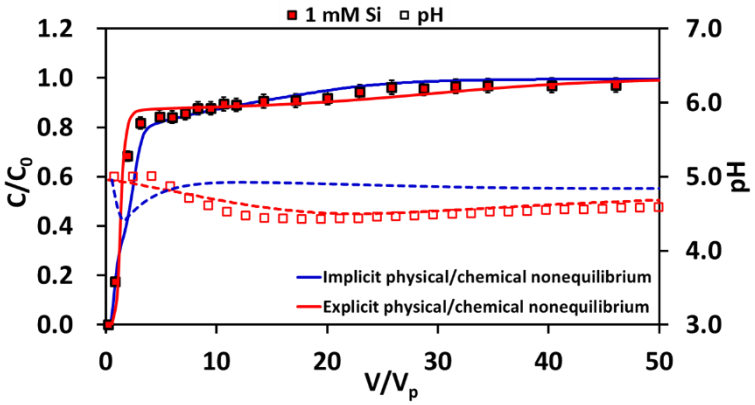

Figure S8. Experimental and modeled BTCs for Si and pH in G_{ag}CS columns. Influent solution of 1 mM Si were injected in step-type concentration boundary condition. Inflow conditions for the two sets of experiment: flow rate 0.5 mL/min, 10 mM NaCl background electrolyte, pore volume =4.1± 0.1 mL, inflow pH 5.0 ± 0.1. The solid line and dashed line are modeled BTCs for selected solutes and pH obtained by using PHREEQC-2, and the points represent the observed data. The red solid and dashed lines are the modeled BTCs explicitly considering the physical and chemical non-equilibrium processes. The blue solid and dashed lines are the modeled BTCs using an overall mass transfer rate coefficient, namely implicit approach.

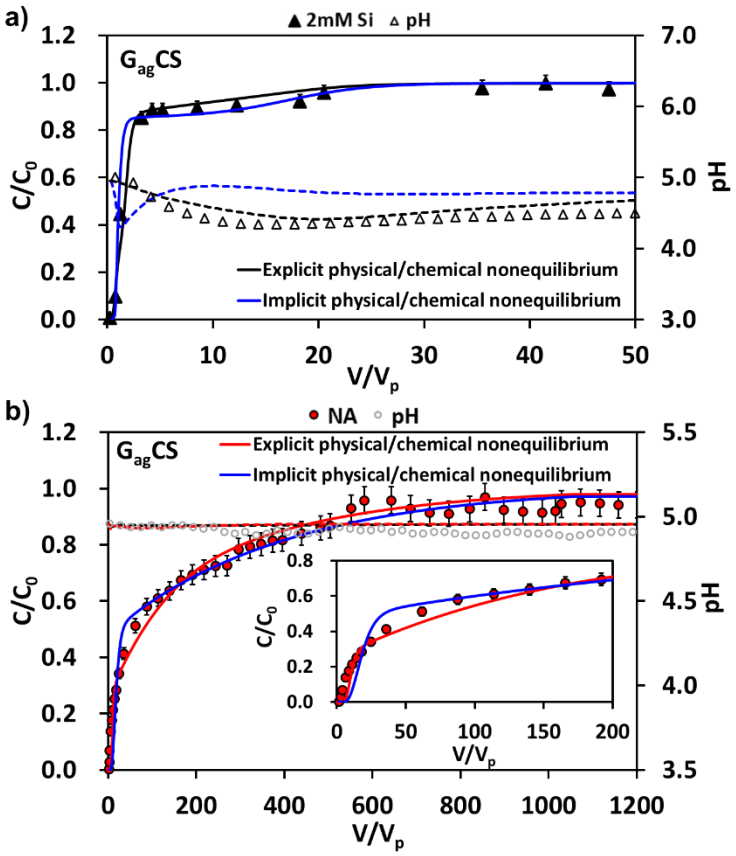

Figure S9. a) Experimental and modeled BTCs for Si and pH in $G_{ag}CS$ columns; influent solution of 2-mM Si were injected in step-type concentration boundary condition. b) Experimental and modeled BTCs for NA and pH in $G_{ag}CS$ columns; influent solutions of 10-µM NA were injected in step-type concentration boundary condition; embedded subfigure: zoom in for V/V_p range of 0–200. Inflow conditions for the two sets of experiment: flow rate 0.5 mL/min, 10-mM NaCl background electrolyte, pore volume =4.1± 0.1 mL, inflow pH 5.0 ± 0.1. The solid line and dashed line are modeled BTCs for selected solutes and pH obtained by using PHREEQC-2. The points represent the observed data. The blue solid and dashed lines are the modeled BTCs using an overall mass transfer rate coefficient–i.e., the implicit approach.

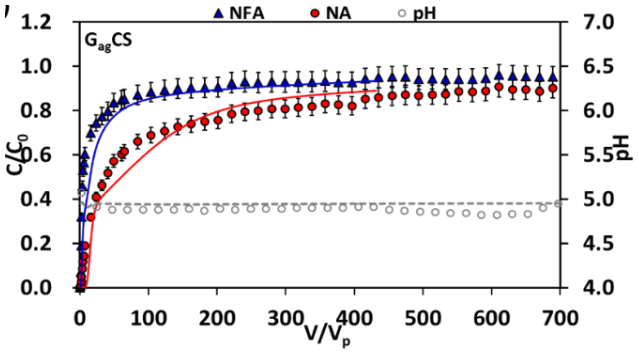

Figure S10. Experimental and modeled BTCs for NA and NFA in $G_{ag}CS$ columns. Inflow conditions: [NA] = 10 µM , [NFA] = 10 µM, flow rate = 0.5 mL/min, 10-mM NaCl background electrolyte, inflow pH 5.0 ± 0.1. Pore volumes is 4.1± 0.1 mL, respectively. Solid lines and dashed lines are modeled BTCs obtained using PHREEQC-2. Points represent the experimental data points.

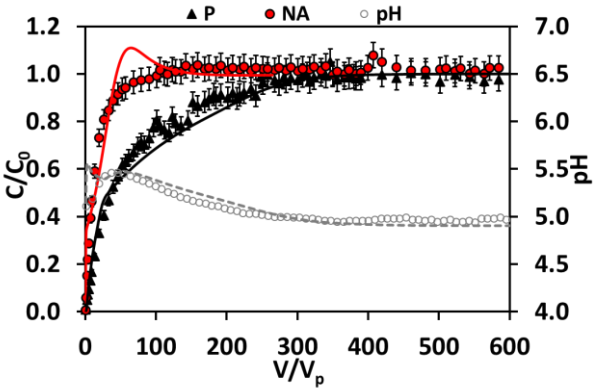

Figure S11. Experimental and modeled BTCs for NA and P in $G_{ag}CS$ columns. Inflow conditions: [NA]= 10 µM, [PO_4] =100 µM, flow rate = 0.5 mL/min, 10 mM NaCl background electrolyte, inflow pH 5.0 ± 0.1. Pore volumes of GCS columns and $G_{ag}CS$ columns are 4.3± 0.1 mL and 4.1± 0.1 mL, respectively. Solid lines and dashed lines are modeled BTCs obtained by using PHREEQC-2, and points represent the experimental data points.

References:

(1) Halasz, I.; Agarwal, M.; Li, R.; Miller, N. Vibrational Spectra and Dissociation of Aqueous Na2SiO3 Solutions. *Catal. Lett.* **2007**, *117* (1), 34–42. https://doi.org/10.1007/s10562-007-9141-6.

(2) Gaboriaud, F.; Ehrhardt, J.-J. Effects of Different Crystal Faces on the Surface Charge of Colloidal Goethite (α-FeOOH) Particles: An Experimental and Modeling Study. *Geochim. Cosmochim. Acta* **2003**, *67* (5), 967–983. https://doi.org/10.1016/S0016-7037(02)00988-2.

(3) Hofmann, A.; Pelletier, M.; Michot, L.; Stradner, A.; Schurtenberger, P.; Kretzschmar, R. Characterization of the Pores in Hydrous Ferric Oxide Aggregates Formed by Freezing and Thawing. *J. Colloid Interface Sci.* **2004**, *271* (1), 163–173. https://doi.org/10.1016/j.jcis.2003.11.053.

(4) Rusch, B.; Hanna, K.; Humbert, B. Coating of Quartz Silica with Iron Oxides: Characterization and Surface Reactivity of Iron Coating Phases. *Colloids Surf. Physicochem. Eng. Asp.* **2010**, *353* (2), 172–180. https://doi.org/10.1016/j.colsurfa.2009.11.009.

(5) Marsac, R.; Martin, S.; Boily, J.-F.; Hanna, K. Oxolinic Acid Binding at Goethite and Akaganéite Surfaces: Experimental Study and Modeling. *Environ. Sci. Technol.* **2016**, *50* (2), 660–668. https://doi.org/10.1021/acs.est.5b04940.

(6) Xu, J.; Marsac, R.; Costa, D.; Cheng, W.; Wu, F.; Boily, J.-F.; Hanna, K. Co-Binding of Pharmaceutical Compounds at Mineral Surfaces: Molecular Investigations of Dimer Formation at Goethite/Water Interfaces. *Environ. Sci. Technol.* **2017**, *51* (15), 8343–8349. https://doi.org/10.1021/acs.est.7b02835.

(7) Parkhurst, D. L.; Appelo, C. A. J. User's Guide to PHREEQC (Version 2): A Computer Program for Speciation, Batch-Reaction, One-Dimensional Transport, and Inverse Geochemical Calculations. *Water-Resour. Investig. Rep.* **1999**, *99* (4259), 312.

(8) Hiemstra, T.; Van Riemsdijk, W. H. A Surface Structural Approach to Ion Adsorption: The Charge Distribution (CD) Model. *J. Colloid Interface Sci.* **1996**, *179* (2), 488–508. https://doi.org/10.1006/jcis.1996.0242.

(9) Kanematsu, M.; Waychunas, G. A.; Boily, J.-F. Silicate Binding and Precipitation on Iron Oxyhydroxides. *Environ. Sci. Technol.* **2018**, *52* (4), 1827–1833. https://doi.org/10.1021/acs.est.7b04098.

(10) Rahnemaie, R.; Hiemstra, T.; van Riemsdijk, W. H. Geometry, Charge Distribution, and Surface Speciation of Phosphate on Goethite. *Langmuir* **2007**, *23* (7), 3680–3689. https://doi.org/10.1021/la062965n.

(11) Hiemstra, T.; Van Riemsdijk, W. H. A Surface Structural Approach to Ion Adsorption: The Charge Distribution (CD) Model. *J. Colloid Interface Sci.* **1996**, *179* (2), 488–508.

(12) van Genuchten, M. Th.; Wagenet, R. J. Two-Site/Two-Region Models for Pesticide Transport and Degradation: Theoretical Development and Analytical Solutions. *Soil Sci. Soc. Am. J.* **1989**, *53* (5), 1303–1310. https://doi.org/10.2136/sssaj1989.03615995005300050001x.

(13) Liu, C.; Zachara, J. M.; Qafoku, N. P.; Wang, Z. Scale-Dependent Desorption of Uranium from Contaminated Subsurface Sediments. *Water Resour. Res.* **2008**, *44* (8). https://doi.org/10.1029/2007WR006478.

(14) Hiemstra, T.; Van Riemsdijk, W. H. On the Relationship between Charge Distribution, Surface Hydration, and the Structure of the Interface of Metal Hydroxides. *J. Colloid Interface Sci.* **2006**, *301* (1), 1–18. https://doi.org/10.1016/j.jcis.2006.05.008.

(15) Rietra, R. P. J. J.; Hiemstra, T.; van Riemsdijk, W. H. Electrolyte Anion Affinity and Its Effect on Oxyanion Adsorption on Goethite. *J. Colloid Interface Sci.* **2000**, *229* (1), 199–206. https://doi.org/10.1006/jcis.2000.6982.

(16) Xu, J.; Marsac, R.; Wei, C.; Wu, F.; Boily, J.-F.; Hanna, K. Cobinding of Pharmaceutical Compounds at Mineral Surfaces: Mechanistic Modeling of Binding and Cobinding of Nalidixic Acid and Niflumic Acid at Goethite

Surfaces. *Environ. Sci. Technol.* **2017**, *51* (20), 11617–11624. https://doi.org/10.1021/acs.est.7b02900.

(17) Hiemstra, T.; Barnett, M. O.; van Riemsdijk, W. H. Interaction of Silicic Acid with Goethite. *J. Colloid Interface Sci.* **2007**, *310* (1), 8–17. https://doi.org/10.1016/j.jcis.2007.01.065.

(18) Das, B. S.; Kluitenberg, G. J. Moment Analysis to Estimate Degradation Rate Constants from Leaching Experiments. *Soil Sci. Soc. Am. J.* **1996**, *60* (6), 1724–1731.

(19) Lassabatere, L.; Winiarski, T.; Galvez-Cloutier, R. Retention of Three Heavy Metals (Zn, Pb, and Cd) in a Calcareous Soil Controlled by the Modification of Flow with Geotextiles. *Environ. Sci. Technol.* **2004**, *38* (15), 4215–4221. https://doi.org/10.1021/es035029s.

(20) Lamy, E.; Lassabatere, L.; Bechet, B.; Andrieu, H. Effect of a Nonwoven Geotextile on Solute and Colloid Transport in Porous Media under Both Saturated and Unsaturated Conditions. *Geotext. Geomembr.* **2013**, *36*, 55–65. https://doi.org/10.1016/j.geotexmem.2012.10.009.

(21) Šimůnek, J.; Genuchten, M. T. van. Modeling Nonequilibrium Flow and Transport Processes Using HYDRUS. *Vadose Zone J.* **2008**, *7* (2), 782–797. https://doi.org/10.2136/vzj2007.0074.

(22) van Genuchten, M. T.; Wierenga, P. J. Mass Transfer Studies in Sorbing Porous Media I. Analytical Solutions 1. *Soil Sci. Soc. Am. J.* **1976**, *40* (4), 473–480. https://doi.org/10.2136/sssaj1976.03615995004000040011x.

(23) Lassabatere, L.; Spadini, L.; Delolme, C.; Février, L.; Galvez Cloutier, R.; Winiarski, T. Concomitant Zn-Cd and Pb Retention in a Carbonated Fluvio-Glacial Deposit under Both Static and Dynamic Conditions. *Chemosphere* **2007**, *69* (9), 1499–1508.

(24) Masciopinto, C.; Passarella, G. Mass-Transfer Impact on Solute Mobility in Porous Media: A New Mobile-Immobile Model. *J. Contam. Hydrol.* **2018**, *215*, 21–28. https://doi.org/10.1016/j.jconhyd.2018.06.004.

(25) Zhou, L.; Cheng, W.; Marsac, R.; Boily, J.-F.; Hanna, K. Silicate Surface Coverage Controls Quinolone Transport in Saturated Porous Media. *J. Colloid Interface Sci.* **2022**, *607*, 347–356. https://doi.org/10.1016/j.jcis.2021.08.142.